Unified drain-current model of complementary p- and n-type OTFTs

Unified drain-current model of complementary p- and n-type OTFTs

Fabrizio Torricelli[1], Matteo Ghittorelli[1], Matteo Rapisarda[2], Antonio Valletta[2], Luigi Mariucci[2], Stephanie Jacob[3], Romain Coppard[3], Eugenio Cantatore[4], Zsolt Miklós Kovács-Vajna[1], Luigi Colalongo[1]

[1]*Department of Information Engineering, University of Brescia, via Branze 38, 25123 Brescia, Italy*

[2]*CNR-IMM, Via del fosso del Cavaliere 100, Roma, Italy*

[3]*CEA-LITEN, 17 rue des martyrs, 38054 Grenoble Cedex 9, France*

[4]*Department of Electrical Engineering, Eindhoven University of Technology, Eindhoven, The Netherlands*

Abstract

A unified drain current model of complementary (p- and n-type) Organic Thin Film Transistors (OTFTs) is presented. The model is physically based and takes into account the detailed properties of the organic semiconductor through the density of states (DOS). The drain current depends on the geometrical and physical parameters of the transistor, on the applied gate, drain and source voltages, and on the surface potential at the source and drain contacts. An analytical expression of the surface potential is derived. The proposed model is validated with the numerical calculations and the measurements of both p- and n-type OTFTs fabricated in a printed complementary technology. The provided analyses show that the model is continuous, accurate, and includes the main physical effects taking place in complementary organic transistors. Thanks to its analytical and symmetric formulation, it is suitable for the design of organic integrated circuits. Moreover, the unified physical picture provided by the model enables the extraction of the OTFTs physical parameters, thus it is a very powerful tool for the technology characterization.

Keywords: Organic thin-film transistor (OTFT), Organic field-effect transistor (OFET), Modelling, Circuit design, Complementary technology

1. Introduction

Organic electronics is growing both at the research and industrial scales. On one side new materials [1], fabrication processes [2], devices [3], sensors [4, 5], and circuits [6] have been developed; while, on the other side, market applications such as active matrix organic light emitting displays (AMOLEDs) [7, 8], and radio-frequency identification tags (RF-ID) [9, 10] are available. The potential of organic technologies is huge: organic semiconductors can be processed at low-temperature and can be easily tailored and optimized for specific applications.

State-of-art organic technologies provide both p- and n-type thin-film transistors printed on large-area flexible substrates, like plastic foils, at temperatures lower than 150°C [11, 12, 13, 14]. Complementary organic thin-film transistors (OTFTs) are the key asset to develop reliable, low-power, fully-organic integrated circuits. Hence, it is expected that complementary OTFT technologies will play the same role of the CMOS technologies for the silicon-based applications. To further improve the performances and the functionalities offered by the OTFT technologies, accurate and physically-based analytical models are essential. They enable to design high-functionality circuits and to move forward the understanding on organic semiconductors and devices.

Email address: fabrizio.torricelli@unibs.it (Fabrizio Torricelli[1])

The performance of organic thin-film transistors is strictly related to the disordered microstructure of the semiconductor [15, 16, 17, 18]. In particular, the structural and energetic disorder of the organic semiconductor (OSC) is reflected in the width and shape of its spectral density of states (DOS) [18, 19, 20]. Although the DOS is material and process dependent [21, 22, 23], several works have shown that in OTFTs the DOS can be approximated by an exponential [24, 25, 26] or a double exponential function [22, 27, 28, 29]. In particular, the former has been mainly observed in p-type OTFTs while the latter has been observed in both p-type and n-type OTFTs. Interestingly, in [29] a double exponential shape of the DOS has been found also in high-mobility ambipolar OTFTs with balanced holes and electrons transport.

In the last years, several analytical OTFT models were proposed [30]-[45]. Basically, they can be divided in two classes: physically-based models that account for the charge transport in the organic DOS [30]-[36] and accurate compact models for circuit simulation [37]-[45]. Although the aforementioned physical and compact models should be valid for both p- and n-type OTFTs, they have been validated on p-type only OTFTs. Therefore, it is not clear what are the physical scenario and the key model parameters required to describe both p- and n-type OTFTs. A unified analytical model based on the physical analysis of complementary OTFT measurements is still missing.

In this work an analytical drain-current and surface-potential

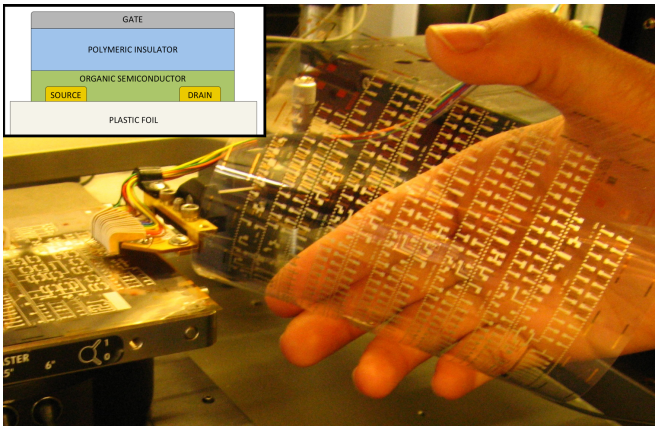

Figure 1: Picture of a 11 cm x 11 cm plastic foil with printed single devices and complementary digital and analog circuits. Inset: cross-section of the OTFTs. The transistor architecture is a bottom-contact top-gate staggered structure.

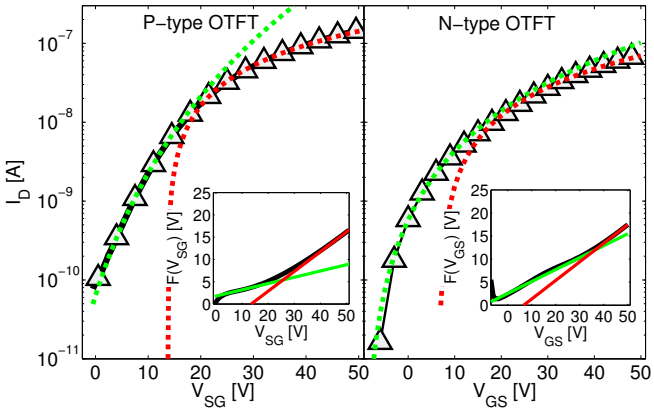

Figure 2: Main Panel: Transfer characteristics of a p-type (left panel) and n-type (right panel) OTFT at $|V_{DS}|$ =0.1V. The black line with symbols are the measured data, the green and red dashed lines accounts for a single exponential DOS only [34]. Insets: the black line is the functional $F(V_G)$, the green and red lines are the fitting at small and large gate voltages, respectively [36].

model for both p-type and n-type OTFTs is proposed. It is derived assuming the charge carriers hopping and it is validated with the numerical calculations and measurements of high-mobility p- and n-type OTFTs fabricated in a printed technology. The provided analysis shows that a double exponential DOS is required to get a unified physical description of complementary OTFTs. The model is accurate, provide physical insight and can be used for circuit simulation and technology characterization.

2. Transistors fabrication and measurements

Organic transistors are fabricated on 11cm x 11cm flexible PEN foil (Fig. 1) using a bottom-contact top-gate structure for both p- and n-type OTFTs. At first, 30 nm thick layer of gold is deposited by sputtering and patterned by photolithography forming the source and drain electrodes [46]. Then, a self-assembled monolayer (SAM) is used to optimize the charge injection in the semiconductor; different SAMs are used for p- and n-type OTFTs. The n-type (Polyera ActiveInk®) and p-type (Merck Lisicon S1200®) OSCs are printed with a thickness of about 100 nm. The gate insulator is a fluoropolymer dielectric (Merck Lisicon D139®) screen-printed on top of both semiconductors and then annealed, leaving open areas for via holes, with a final thickness of 750 nm. Finally, a silver-ink conductor is screen-printed on the top of the dielectric and annealed at 100°C, forming in the same step the gate electrodes for devices and the second level for interconnections. The transistors are measured in air at room temperature.

3. Preliminary analysis: Density of states

The measured transfer characteristics of a p- and n-type OTFT are shown in Fig. 2. In order to assess if a single exponential or a double exponential function is required to model the DOS of complementary OTFTs, the functional [36, 47] $F(V_G) = \int_0^{V_G} I_D(V_g)dV_g/I_D(V_G)$ is calculated. The results are shown in the insets of Fig. 2 (black line). In both p- and n-OTFTs the functional $F(V_G)$ is not a straight line but, instead, it can be approximated by two straight lines. Each line corresponds to an exponential distribution of energy states: the green line is for the deep states while the red line is for the tail states. Therefore, according to the analysis proposed in [36], a double exponential DOS is required:

$$g(E) = \frac{N_d}{k_B T_d} \exp\left(\frac{E - E_0}{k_B T_d}\right) + \frac{N_t}{k_B T_t} \exp\left(\frac{E - E_0}{k_B T_t}\right) \quad (1)$$

where N_d, N_t, and T_d, T_t, are the total density of states and the characteristic temperatures of deep and tail states, respectively. E_0 is the reference energy, and it corresponds to the highest/lowest occupied/unoccupied molecular orbital (HOMO/LUMO) for holes/electrons, respectively.

Interestingly, in the p-OTFT (inset of Fig. 2 - left panel) the deep and tail distributions cross at about $V_{SG} = 25V$, the transition is very sharp and at large V_G the deep states are much less than the tail states. On the other hand, in the n-OTFT (inset of Fig. 2 - right panel) the deep and tail distributions cross at about $V_{GS} = 37V$, and the transition from one region to the other is quite slow.

The impact of the DOS shape is readily visible on the drain current. In the main panels of Fig. 2 the drain currents calculated with only the deep states (dashed green line) and only the tail states (dashed red line) are compared with the measured currents. At low gate voltages, corresponding to low carriers energy, the Fermi level moves down to the deep states that are responsible of the weak-accumulation current. This holds for both p- and n-OTFTs.

When the gate voltage increases, the Fermi level is pushed at higher energies. In p-OTFTs the strong accumulation current ($V_{SG} > 25V$) depends on the tail states only, and the transition region from deep-to-tail states is very sharp. On the other hand, in the n-OTFTs the deep and tail states are comparable,

the transition region extends for a wide range of gate voltages ($20V < V_{GS} < 50V$) and the strong accumulation current is defined by both the deep and tail states.

In order to reproduce the drain current in the whole range of gate voltages, a continuous model accounting for both deep and tail states is required. A simple approach was proposed in [36] but unfortunately it is accurate only when the transition from deep to tail states is sharp. As shown in Fig. 2 this requirement is fulfilled only for p-type OTFTs.

In the following an accurate analytical model able to overcome this limitation is presented: it is an unified physical description valid for both p- and n-type OTFTs.

4. Drain-current OTFT model

For the sake of simplicity, in the following the model will be derived for n-type OTFTs, and same considerations hold for p-type OTFTs. The integral expression of the drift-diffusion current reads [34]:

$$I_{DS} = \frac{W}{L}\int_{V_S}^{V_D}\int_{V_{ch}}^{\varphi_s}\frac{\sigma(\varphi, V_{ch})}{F_x(\varphi, V_{ch})}d\varphi dV_{ch} \tag{2}$$

where W is the channel width, L is the channel length, V_S and V_D are the source and the drain voltages, respectively, V_{ch} is the channel potential (viz. the pseudo Fermi energy), φ is the electrostatic potential and φ_s is the surface potential at the insulator-semiconductor interface. σ is the variable range hopping conductivity, that in the case of a double exponential DOS reads [48]: $\sigma = S_0 \exp\left[q(\varphi - V_{ch})/(k_B T)\right]$, where $S_0 = \sigma_0[\pi N_t T_t^3/(8\alpha^3 B_c T^3)]^{T_t/T} \exp\left[\Delta E_{Fi}/(k_B T)\right]$ is a function of the organic semiconductor parameters ($B_c = 2.8$, $\alpha^{-1} = 2.2$Å), and $\Delta E_{Fi} = E_{gap}/2 - E_0$.

The electric field in the x-direction $F_x(\varphi, V_{ch})$ is calculated with the Poisson equation $\nabla^2\varphi = -(\partial F_x/\partial x + \partial F_y/\partial y)$ and assuming the gradual channel approximation (i.e. $F_x \gg F_y$) results:

$$F_x(\varphi, V_{ch}) = \sqrt{\frac{2q}{\epsilon_s}\int_{V_{ch}}^{\varphi} n(\varphi', V_{ch})d\varphi'} \tag{3}$$

$$\simeq \sqrt{\frac{2q}{\epsilon_s}\left[k_d e^{\frac{q(\varphi - V_{ch})}{k_B T_d}} + k_t e^{\frac{q(\varphi - V_{ch})}{k_B T_t}}\right]} \tag{4}$$

where $\epsilon_s = \epsilon_0 k_s$, ϵ_0 is the vacuum permittivity, k_s is the semiconductor relative permittivity, and $n = \int g(E) f(E; E_F) dE$ is the charge concentration given by the Fermi-Dirac integral solved for the DOS distribution in Eq. 1. k_d and k_t are calculated as $k_o = (N_o \vartheta_o k_B T_o/q) \exp\left[\Delta E_{Fi}/(k_B T_o)\right]$, $o \in \{d, t\}$, and $\vartheta_o = \pi(T/T_o)/\sin(\pi T/T_o)$ because in our case $T_o > T$ [49]. It is worth noting that k_d and k_t depend only on the DOS parameters and on the temperature T.

Since the electric field (Eq. 4) is the sum of two exponential functions, Eq. 2 cannot be solved analytically. To this aim, the electric field can be re-written as a single exponential function by means of the effective temperature approach [50], and Eq. 4 can be written as $F_x(\varphi, V_{ch}) = F_0 \exp\left[q(\varphi - V_{ch})/(2k_B T_e)\right]$, where $F_0 = \sqrt{2q(k_d + k_t)/\epsilon_s}$, and the effective temperature reads:

$$T_e(\varphi, V_{ch}) = \frac{q(\varphi - V_{ch})}{2k_B \log\left[\frac{F_x(\varphi, V_{ch})}{F_0}\right]} \tag{5}$$

Eq. 5 accounts for both deep and tail states: it depends on the DOS parameters (viz. N_d, N_t and T_d, T_t). At small charge carrier concentrations the effective temperature is close to the characteristic temperature of the deep states T_d, whereas when the Fermi level is pushed at high energy by the gate voltage (large carriers concentrations), the effective temperature is close to the characteristic temperature of the tail states T_t.

Replacing Eq. 5 in Eq. 2 and integrating with respect to $d\varphi$, the drain current reads:

$$I_{DS} \simeq \frac{W}{L}\frac{S_0 E_\delta}{qF_0}\int_{V_S}^{V_D}\exp\left[\frac{q(\varphi_s - V_{ch})}{E_\delta}\right]dV_{ch} \tag{6}$$

where $E_\delta = 2k_B T T_e/(2T_e - T)$. To work out an analytical expression of the drain current (6) an expression of the surface potential φ_s is required. By applying Gauss' law to the insulator-semiconductor interface, one obtains:

$$F_x(\varphi_s, V_{ch}) = \frac{C_i}{\epsilon_s}(V_{GF} - \varphi_s) \tag{7}$$

where C_i is the gate capacitance per unit area, $V_{GF} = V_G - V_{FB}$, V_G and V_{FB} are the gate and the flatband voltages, respectively. Replacing Eq. 5 in Eq. 7 the band bending $(\varphi_s - V_{ch})$ is calculated as a function of the gate voltage:

$$\varphi_s - V_{ch} = 2k_B T_e \log\left[\frac{C_i}{\epsilon_s F_0}(V_{GF} - \varphi_s)\right] \tag{8}$$

After substituting Eq. 8 in Eq. 6 and changing the integration variable from dV_{ch} to $d\varphi_s$ [34], the drain current turns out to be:

$$I_{DS} = \frac{W}{L}\left[\beta_S (V_{GF} - \varphi_{sS})^{\gamma_S} - \beta_D (V_{GF} - \varphi_{sD})^{\gamma_D}\right] \tag{9}$$

where

$$\beta_\chi = \frac{k_B T}{q}\frac{S_0}{\gamma_\chi - 1}\left(\frac{C_i}{\epsilon_s}\right)^{\gamma_\chi - 1}\left[\frac{2q}{\epsilon_s}(k_d + k_t)\right]^{-\frac{\gamma_\chi}{2}}$$

$$\gamma_\chi = \frac{2T_{e\chi}/T}{\log\left[k_d \exp\left(\frac{T_{e\chi}}{T_d}\right) + k_t \exp\left(\frac{T_{e\chi}}{T_t}\right)\right] - \log\left[k_d + k_t\right]}$$

$$T_{e\chi} = \frac{q}{k_B}\left(\varphi_{s\chi} - V_\chi\right)$$

$\chi \in \{S, D\}$, and φ_{sS}, φ_{sD} is the surface potential calculated at the source and the drain contact, respectively.

The analytical drain-current model (Eq. 9) is valid when the DOS shape in the organic layer of the transistor can be approximated by the sum of two exponential functions and it accurately reproduces the transition from deep to tail energy states. β_χ and γ_χ are functions of the tail and deep DOS parameters (viz. N_t, T_t, N_d, T_d), of the pseudo-Fermi potential V_χ, and of the surface potential φ_χ at the source and drain. As a result, β_χ and γ_χ vary with the applied voltages: at small V_G (small concentrations) they basically depend on the deep states only, at large V_G (large

concentrations) they basically depend on the tail states only, and in the transition region β_χ and γ_χ depend on both the deep and tail states. Thanks to this approach, the proposed model is simple and, at the same time, it accurately accounts for the charge transport in a double-exponential DOS.

The surface potential in Eq. 9 has to be calculated by solving the non linear Gauss equation (Eq. 7 where F_x is given by Eq. 4) at the semiconductor/insulator interface:

$$\frac{C_i}{\sqrt{2q\epsilon_s}}(V_{GF}-\varphi_s)=\sqrt{k_d e^{\frac{q(\varphi_s-V_{ch})}{k_B T_d}}+k_t e^{\frac{q(\varphi_s-V_{ch})}{k_B T_t}}} \qquad (10)$$

It is worth noting that Eq. 10 can only be solved by numerical iterations.

5. Surface potential model

In order to derive an analytical approximation of Eq. 10 we observe that:

1. In subthreshold or saturation $V_{GF}-V_{ch}\leq 0$, and the surface potential reads:

$$\varphi_s = V_{GF} \qquad (11)$$

2. In linear region $V_{GF}-V_{ch}>0$, the right-hand-side of Eq. 10 can be approximated as $(V_{GF}-\varphi_s)\simeq(V_{GF}-V_{ch})$ and Eq. 10 reads:

$$\frac{C_i^2}{2q\epsilon_s}(V_{GF}-V_{ch})^2 \simeq k_d\, e^{\frac{q(\varphi_s-V_{ch})}{k_B T_d}}+k_t\, e^{\frac{q(\varphi_s-V_{ch})}{k_B T_t}}$$

that, in turn, can be reworked out as: $F_\perp = k_d\, u^{\frac{T_t}{T_d}}+k_t\, u$, where

$$F_\perp = \left[C_i\,(V_{GF}-V_{ch})\right]^2/(2q\epsilon_s) \qquad (12)$$

and $u=\exp\left[q(\varphi_s-V_{ch})/k_B T_t\right]$. After straightforward manipulations one obtains:

$$\left(1-\frac{k_t}{F_\perp}u\right)^{\frac{T_d}{T_t}}=\left(\frac{k_d}{F_\perp}\right)^{\frac{T_d}{T_t}}u \qquad (13)$$

Since $k_t\,u/F_\perp << 1$ the left hand side of Eq. 13 can be accurately approximated by the second order Taylor expansion:

$$\frac{k_t^2}{2F_\perp^2}\frac{T_d^2-T_dT_t}{T_t^2}u^2-\left[\frac{T_d}{T_t}\frac{k_t}{F_\perp}+\left(\frac{k_d}{F_\perp}\right)^{\frac{T_d}{T_t}}\right]u+1=0$$

Solving with respect to the variable u results:

$$u=\frac{2F_\perp T_t\left(k_t T_d+F_\perp T_t\left(\frac{k_d}{F_\perp}\right)^{\frac{T_d}{T_t}}\right)^{-1}}{1+\sqrt{1+\frac{2k_t^2T_d(T_d-T_t)}{\left[k_tT_d+F_\perp T_t\left(\frac{k_d}{F_\perp}\right)^{\frac{T_d}{T_t}}\right]^2}}} \qquad (14)$$

and the surface potential eventually reads:

$$\varphi_s = V_{ch}+k_B T_t\log(u) \qquad (15)$$

In Fig. 3 the analytical approximation (Eqs. 11 and 15) is compared with the exact numerical solution of Eq. 10 as a function of the gate voltage V_{GF} and of the typical DOS parameters T_d/T_t. The surface potential model is very accurate in the whole range of gate voltages and DOS parameters. The maximum error is smaller than 6% and it becomes smaller than 2% few volts above the flat-band voltage (i.e. $V_{GF}>3V$).

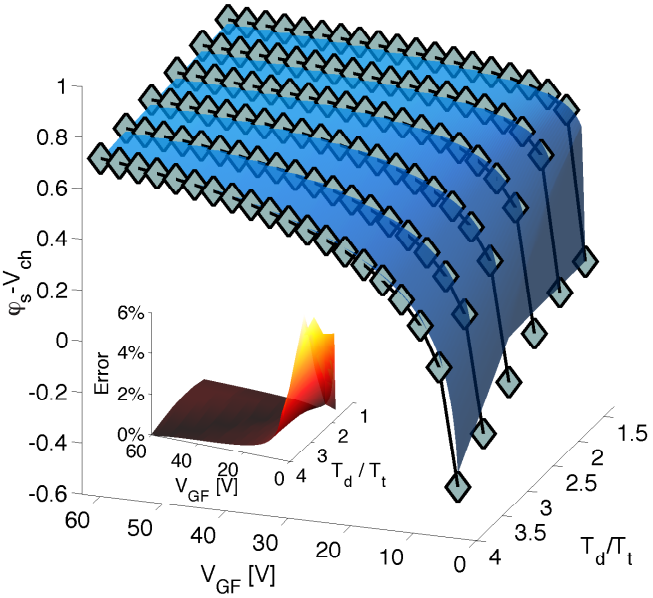

Figure 3: Main Panel: Numerical solution of the surface potential (line with symbols) vs. approximate solution Eq. 15 (surface) as a function of V_{GF} and T_d/T_t. Inset: percentage error $100\times|Eq.15-Eq.10|/Eq.10$ as a function of V_{GF} and T_d/T_t.

6. Results and Discussion

The measured transfer and output characteristics of both p-type and n-type OTFTs are compared with the proposed analytical model (Eqs. 9, 11, and 15) in Figs. 4, 5, and 6, respectively. There is a good agreement between the measurements and the model in the whole range of bias conditions. The model is continuous and accounts for all the OTFT operating regions, i.e. strong accumulation, weak accumulation and sub-threshold.

More in detail, in case of p-type OTFTs the model accurately predicts both the transfer and output characteristics, while in case of the n-type OTFTs the model slightly overestimates the current at large drain voltages. This is evident from the output characteristics shown in Fig. 6 and, according to several studies [51, 52, 53, 54], we verified that it is due to the parasitic contact resistance at the source injecting contact. This is further confirmed by the normalized transfer characteristics shown in Fig. 7: scaling down the transistors channel length the model (full line) overestimates the L/W-normalized current only at large drain voltages. The contact resistance is larger in n-type OTFTs and it is due to the energy barrier at the metal-semiconductor contact. Indeed, in p-OTFTs (Fig. 7 left panel)

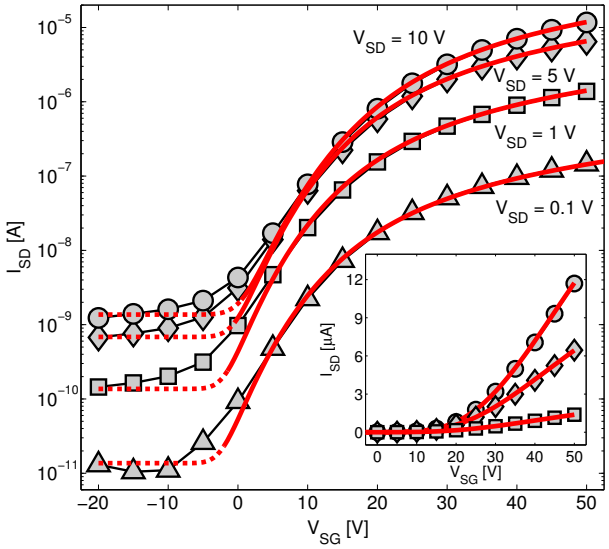

Figure 4: Transfer characteristics of a p-type OTFT at various drain-source voltages. Black lines with symbols are the measurements and red lines are the model. Dashed line is the leakage current calculated with $R_{off} = (W/L)(V_{DS}/I_D)$. The geometrical and physical parameters are listed in Table 1.

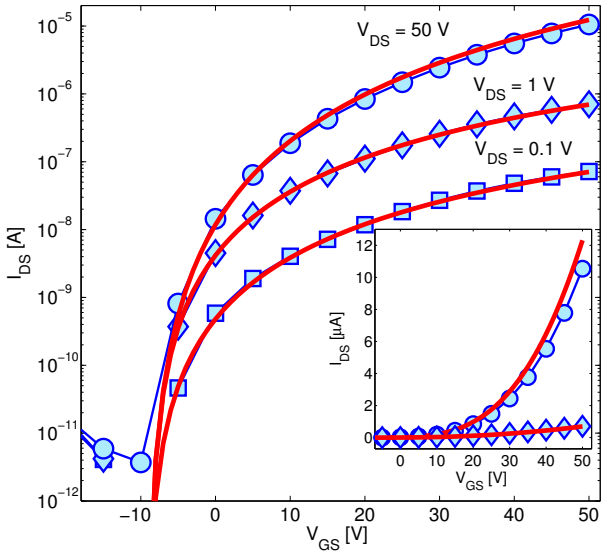

Figure 5: Transfer characteristics of a n-type OTFT at various drain-source voltages. Black lines with symbols are the measurements and red lines are the model. The geometrical and physical parameters are listed in Table 1.

with $L = 200\mu m$, and $L = 100\mu m$ the model (full line) perfectly agrees with the measurements in the whole range of drain voltages. When the channel length is $L = 50\mu m$ the model accurately predicts the transistor current only at low drain voltages ($V_{SD} < 5V$), while the current is overestimated at larger drain voltages and at smaller channel lengths (i.e. $L = 20\mu m$ and $L = 10\mu m$). The same considerations hold in case of n-OTFTs (Fig. 7 right panel) where the contact resistance limits the drain current at larger channel lengths compared to the p-OTFTs. It should be pointed out that the larger contact resistance of n-OTFTs reduces the leakage current in the bulk of the semiconductor (see the off-region in Figs 4, 5). In the case of the p-OTFTs the leakage current as a function of the drain voltage can be reproduced by $I_{leak} = (W/L)(V_{DS}/R_{off})$.

This analysis shows that the contact resistance cannot be neglected. It can be easily included in the model following the approaches [51, 55, 56, 57, 58]. The idea is to split the channel into a small contact region, where there is a voltage drop V_C, and the main channel, where the voltage drop is $V_{DS} - V_C$. In other words, the channel potential at the source side is $V_S + V_C$ instead of V_S. In Fig. 7 the L/W-normalized drain current of p- and n-OTFTs at different channel lengths is calculated (dashed lines) with the proposed model (Eqs. 9, 11, and 15) and the voltage drop at the source contact is obtained with the contact model proposed in [51, 56]:

$$I_{DS} = WI_0 \exp\left(\sqrt{\frac{V_C}{V_0}}\right)\left[\exp\left(-\frac{qV_C}{\eta k_B T}\right) - 1\right] \qquad (16)$$

where $I_0 = I_{00}\{\log[1 + \exp(V_{GF}/V_{00})]\}^\theta$, V_0 accounts for the Schottky barrier lowering effect, $\eta = 2$ is the quality factor, and I_0 is the reverse current at $V_C = 0V$. $V_{00} = 1V$ and it is introduced to keep the dimensionality of the pre-factor I_{00}, and θ is

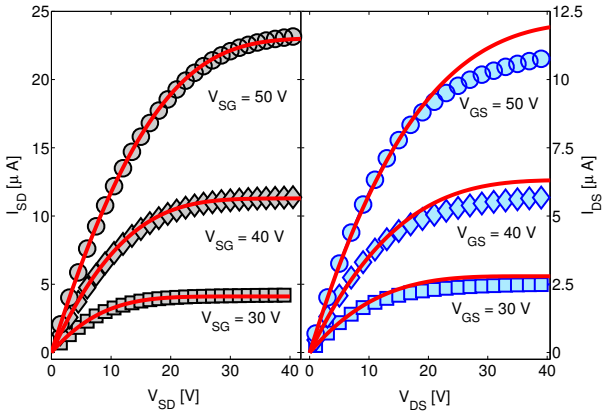

Figure 6: Output characteristics of p-type (left panel) and n-type (right panel) OTFTs at various gate voltages. Symbols are the measurements and red lines are the model. Geometrical and physical parameters are listed in Table 1.

a fitting parameter. As shown in Fig. 7 the overall model (channel+contact) scales with the transistors channel length for both p- and n-OTFTs. It is worth noting that effect of the channel length modulation is weak because in short-channel OTFTs the drain current is limited by the contact. Therefore, the channel length modulation is not included in the model.

The model parameters are listed in Tab. 1. The channel parameters are obtained by means of a single transfer characteristic measured at the minimum drain voltage ($|V_{DS}| = 0.1V$) and for long-channel OTFTs ($L = 200\mu m$). In such conditions the contact resistance is negligible [51, 53, 59] and the model returns the physical parameters of the organic semiconductor (viz. N_t, N_d, T_t, and T_d). The contact parameters (viz. I_{00}, V_0, and θ) are obtained form the output characteristics of short-channel OTFTs ($L = 10\mu m$).

Comparing the extracted parameters of p- and n-type OTFTs,

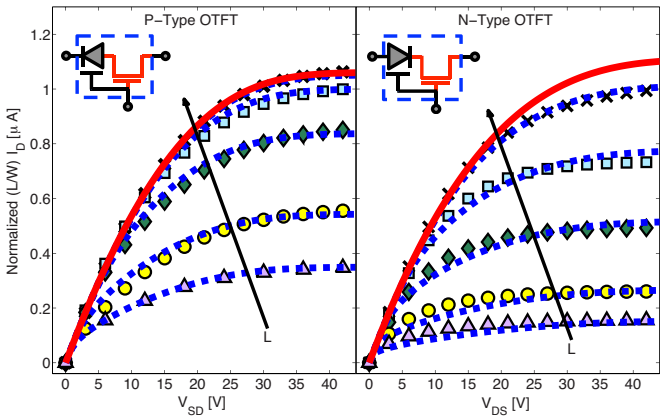

Figure 7: L/W normalized output characteristics of p- and n-type OTFTs. Symbols are the measurements, the red line is the model without taking into account the contact effects (Eqs. 9, 11, and 15), and the blue dashed lines are given by the model taking into account the contact effects (Eqs. 9, 11, 15, and 16). × is $L = 200\mu m$, □ is $L = 100\mu m$, ◇ is $L = 50\mu m$, ◯ is $L = 20\mu m$, and △ is $L = 10\mu m$. $V_{SG} = V_{GS} = 50V$. Inset: equivalent circuit model of the OTFT. The geometrical and physical parameters are given in Table 1.

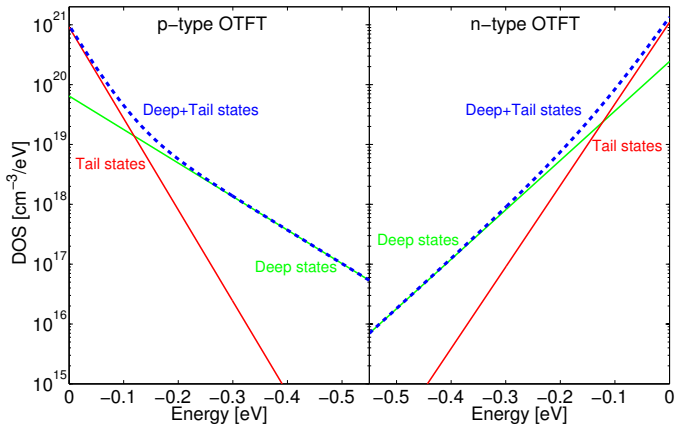

Figure 8: Extracted DOS of p-type and n-type OTFTs. Parameters are listed in Table 1.

one can see that the transistors show the same field-effect mobility and similar values of flat-band voltage V_{FB}, total density of tail states N_t and tail-states characteristic temperature T_t. On the other hand, the total density of deep states N_d in n-type OTFTs is three times larger than that in p-type OTFTs. This explains why the maximum (L/W-normalized) drain current in the n-type OTFT is basically the same of that measured in the p-type OTFT (Fig. 6) although the conductivity pre-factor σ_0 is more than the double. Indeed, the larger number of trap states reduce the overall transistor conductance since they do not contribute to the charge transport [48]. These additional trap states can be attributed to the structural properties of the n-type organic semiconductor and/or to the lower-quality of the n-type OSC-insulator interface [36, 60, 61]. Such information can be exploited to further improve the OTFTs performance, providing an optimized technology for complementary logic circuits.

The extracted DOS of both p- and n-type OSCs are shown in Fig. 8. In the p-type OTFTs the double exponential DOS shows

Table 1: Geometrical and physical parameters of the transistors. W is the channel width, L is the channel lenght, k_s is the permittivity of the organic semiconductor, C_i is the gate-insulator capacitance per unit area, T is the temperature, and μ_{FE} is the field-effect mobility calculated at $|V_{DS}| = 0.1V$, σ_0 is the conductivity prefactor, N_t is the total number of tail-states, N_d is the total number of deep-states, T_t is the tail-states characteristic temperature, T_d is the deep-states characteristic temperature, V_{FB} is the flatband voltage, V_0 accounts for the Schottky barrier lowering, I_{00} is the reverse current pre-factor, θ is a fitting parameter, and R_{off} accounts for the leakage current in the p-type OTFTs.

	P-Type	N-Type
$W\ [\mu m]$	4000	2250
$L\ [\mu m]$	$200 \rightarrow 10$	$200 \rightarrow 10$
k_s	3	3
$C_i\ [nF/cm^2]$	2.2	2.2
$T\ [K]$	295	295
$\mu_{FE}\ [cm^2/Vs]$	1	1
$\sigma_0\ [S/cm]$	8.6×10^5	2.2×10^6
$N_t\ [cm^{-3}]$	1×10^{19}	1.2×10^{19}
$N_d\ [cm^{-3}]$	3.3×10^{18}	8.7×10^{18}
$T_t\ [K]$	330	370
$T_d\ [K]$	940	630
$V_{FB}\ [V]$	9.3	-10.2
$V_0\ [V]$	0.35	1.1
$I_{00}\ [pA/cm]$	400	1.3
θ	2.7	4
$R_{off}\ [G\Omega]$	160	0

two distinct regions: one is dominated by the deep states and the other by the tail states with a sharp transition at about $-0.15eV$ far from the HOMO energy ($E_{HOMO} = 0eV$). In the n-type OTFTs the transition from the deep-states to the tail-states region is rather smooth and, at a first sight, the overall double exponential DOS could be approximated by a single exponential function. The reason is that $N_d/T_d \simeq N_t/T_t$ and therefore the contribution of the tail states is relevant only at energies close to the LUMO level, that are accessed only at very high gate voltages ($V_{GS} > 40V$, i.e. $E_F > -0.1eV$). This perfectly agrees with the preliminary analysis reported in Sec. 3 and gives a unified physical scenario for both holes and electrons transport in organic transistors.

7. Conclusion

In this work an analytical model of p- and n- type OTFTs is proposed. According to the measurements of OTFTs fabricated in a printed complementary technology, the model takes into account a double exponential DOS, which is required to achieve a unified physical description of complementary OTFTs.

The drain current depends on the geometrical and physical parameters of the transistor, on the applied gate, drain and source voltages, and on the surface potential at the source and drain contacts. An analytical expression of the surface potential accounting for a double exponential DOS is derived. The model is validated with both numerical calculations and measurements.

The DOS parameters are calculated by means of the transfer characteristic of long-channel OTFTs. The p- and n-OTFTs show similar mobility, flat-band voltage, and tail states DOS parameters. On the other hand, the n-type OTFTs show a larger number of deep states compared to the p-type OTFTs which reflects in a lower overall conductance of n-OTFTs.

The shape of the measured transfer characteristics is related to the DOS parameters. In the case of our complementary technology, the p-OTFTs show a sharp transition from the deep states to the tail states, while for n-OTFTs the transition is smooth. The proposed model provides a unified description of both the situations. The analysis also shows that the contact resistance due to the charge injection at the source must be taken into account to describe complementary OTFTs with short channel lengths ($L < 50\mu m$ in our technology).

The model can be used for circuit design, technology characterization and process optimization.

Acknowledgments

This work was partially funded in the frame of the European FP7 project COSMIC (grant agreement no. 247681).

8. References

[1] H. Yan, Z. Chen, Y. Zheng, C., Newman, J.R. Quinn, F. Dötz, M. Kastler, A. Facchetti, A high-mobility electron-transporting polymer for printed transistors, Nature 457 (2009) 679-686.

[2] T. Sekitani, U. Zschieschang, H. Klauk, T. Someya, Flexible organic transistors and circuits with extreme bending stability, Nat. Materials 9 (2010) 1015-1022.

[3] M.A. McCarthy, B. Liu, E.P. Donoghue, I. Kravchenko, D.Y. Kim, F. So, A.G. Rinzler, Low-Voltage, Low-Power, Organic Light-Emitting Transistors for Active Matrix Displays, Science 332 (2011) 570-573.

[4] T. Someya, A. Dodabalapur, J. Huang, K.C. See, H.E. Katz, Chemical and Physical Sensing by Organic Field-Effect Transistors and Related Devices, Adv. Mater. 22 (2010) 3799-3811.

[5] G.H. Gelinck, A. Kumar, D. Moet, J.-L. der Steen, U. Shafique, P. E. Malinowski, K. Myny, B.P. Rand, M. Simon, W. Rütten, A. Douglas, J. Jorritsma, P. Heremans, R. Andriessen, X-ray imager using solution processed organic transistor arrays and bulk heterojunction photodiodes on thin, flexible plastic substrate, Organic Electron. 14 (2013) 2602-2609.

[6] M. Kaltenbrunner, T. Sekitani, J. Reeder, T. Yokota, K. Kuribara, T. Tokuhara, M. Drack, R. Schwödiauer, I. Graz, S. Bauer-Gogonea, S. Bauer, T. Someya, An ultra-lightweight design for imperceptible plastic electronics, Nature 499 (2013) 458-463.

[7] Soeren Steudel, K. Myny, S. Schols, P. Vicca, S. Smout, A. Tripathi, B. van der Putten, J.-L. van der Steen, M. van Neer, F. Schütze, O.R. Hild, E. van Veenendaal, P. van Lieshout, M. van Mil, J. Genoe, G. Gelinck, P. Heremans, Design and realization of a flexible QQVGA AMOLED display with organic TFTs, Organic Electron. 13 (2012) 1729-1735.

[8] G.S. Ryu, J.S. Kim, S.H. Jeong, C.K. Song, A printed OTFT-backplane for AMOLED display, Organic Electron. 14 (2013) 1218-1224.

[9] E. Cantatore, T.C.T. Geuns, G.H. Gelinck, E. van Veenendaal, A. Gruijthuijsen, L. Schrijnemakers, S. Drews, and D.M. de Leeuw, A 13.56-MHz RFID system based on organic transponders, IEEE J. Solid-State Circuits 42 (2007) 84-92.

[10] K. Myny, S. Steudel, S. Smout, P. Vicca, F. Furthner, B. van der Putten, A.K. Tripathi, G.H. Gelinck, J. Genoe, W. Dehaene, P. Heremans, Organic RFID transponder chip with data rate compatible with electronic product coding, Organic Electron. 11 (2010) 1176-1179.

[11] M. Guerin, A. Daami, S. Jacob, E. Bergeret, E. Benevent, P. Pannier, R. Coppard, High-Gain Fully Printed Organic Complementary Circuits on Flexible Plastic Foils, IEEE Trans. Electron Devices 58 (2011) 3587-3593.

[12] W. Smaal, C. Kjellander, Y. Jeong, A. Tripathi, B.V.D. Putten, A. Facchetti, H. Yan, J. Quinn, J. Anthony, K. Myny, W. Dehaene, G. Gelinck, Complementary integrated circuits on plastic foil using inkjet printed n- and p-type organic semiconductors: Fabrication, characterization, and circuit analysis, Organic Electron. 13 (2012) 1686-1692.

[13] Y. Takeda, Y. Yoshimura, Y. Kobayashi, D. Kumaki, K. Fukuda, S. Tokito, Integrated circuits using fully solution-processed organic TFT devices with printed silver electrodes, Organic Electron. 14 (2013) 3362-3370.

[14] S. Jacob, S. Abdinia, M. Benwadih, J. Bablet, I. Chartier, R. Gwoziecki, E. Cantatore, A.H.M. Van Roermund, L. Maddiona, F. Tramontana, G. Maiellaro, L. Mariucci, M. Rapisarda, G. Palmisano, R. Coppard, High performance printed N and P-type OTFTs enabling digital and analog complementary circuits on flexible plastic substrate, Solid-State Electron. 84 (2013) 167-178.

[15] F. Torricelli, L. Colalongo, L. Milani, Z.M. Kovács-Vajna, E. Cantatore, Impact of energetic disorder and localization on the conductivity and mobility of organic semiconductors, Proc. Inter. Conf. on Simulation of Semiconductor Processes and Devices P15 (2011) 195-198.

[16] J.J. Brondijk, M. Spijkman, F. Torricelli, P.W.M. Blom, D.M. de Leeuw, Charge transport in dual-gate organic field-effect transistors, Appl. Phys. Lett. 100 (2012) 023308.

[17] P. Kumar, A. Sharma, S. Yadav, S. Ghosh, Morphology optimization for achieving air stable and high performance organic field effect transistors, Organic Electronics 14 (2013) 16631672.

[18] O. Simonetti, L. Giraudet, D. Bugnot, Effective mobility in amorphous organic transistors: Influence of the width of the density of states, Organic Electronics 15 (2014) 35-39.

[19] O. Tal, Y. Rosenwaks, Y. Preezant, N. Tessler, C. K. Chan, and A. Kahn, Direct determination of the hole density of states in undoped and doped amorphous organic films with high lateral resolution, Phys. Rev. Lett. 95 (2005) 256405.

[20] F. Torricelli, Z.M. Kovács-Vajna, L. Colalongo, The role of the density of states on the hole mobility of disordered organic semiconductors, Organic Electron. 10 (2009) 1037-1040.

[21] J. Puigdollers, A. Marsal, S. Cheylan, C. Voz, and R. Alcubilla, Density of-states in pentacene from the electrical characteristics of thin-film transistors, Organic Electron. 11 (2010) 1333-1337.

[22] J. Puigdollers, M. Della Pirriera, A. Marsal, A. Orpella, S. Cheylan, C. Voz, and R. Alcubilla, N-type PTCDI- C13H27 thin-film transistors deposited at different substrate temperature, Thin-Solid Films 517 (2009) 6271-6274.

[23] W.S.C. Roelofs, S.G.J. Mathijssen, R.A.J. Janssen, D.M. de Leeuw, M. Kemerink, Accurate description of charge transport in organic field effect transistors using an experimentally extracted density of states, Phys. Rev. B 85 (2012) 085202.

[24] M.C.J.M. Vissenberg, and M. Matters, Theory of the field-effect mobility in amorphous organic transistors, Phys. Rev. B 57 (1998) 12964-12967.

[25] F. Torricelli, Z.M. Kovács-Vajna, L. Colalongo, A charge control analytical model for organic thin film transistors, Appl. Phys. Lett. 92 (2008) 113306-1-113306-3.

[26] S. Sambandan, R.J.P. Kist, R. Lujan, T. Ng, A.C. Arias, R.A. Street, Compact model for forward subthreshold characteristics in polymer semiconductor transistors, J. Appl. Phys. 106 (2009) 084501-1-084501-8.

[27] F. De Angelis, L. Mariucci, S. Cipolloni, and G. Fortunato, Analysis of electrical characteristics of high performance pentacene thin-film transistors with PMMA buffer layer, J. Non-Crystalline Solids 352 (2006) 1765-1768.

[28] J. Jang, J. Kim, M. Bae, J. Lee, D.M. Kim, D.H. Kim, J. Lee, B.-L. Lee, B. Koo, Y.W. Jin, Extraction of the sub-bandgap density-of-states in polymer thin-film transistors with the multi-frequency capacitance-voltage spectroscopy, Appl. Phys. Lett. 100 (2012) 133506-1-133506-5.

[29] T.-J. Ha, P. Sonar, B. Cobb, A. Dodabalapur, Charge transport and density of trap states in balanced high mobility ambipolar organic thin-film transistors, Organic Electron. 13 (2012) 136-141.

[30] G. Horowitz, P. Delannoy, An analytical model for organic-based thin-film transistors, J. Appl. Phys.70 (1991) 469-475.

[31] L. Torsi, A. Dodabalapur, H. E. Katz, An analytical model for short-channel organic thin-film transistors, J. Appl. Phys. 78 (1995) 1088-1093.

[32] P. Stallinga, H. L. Gomes, F. Biscarini, M. Murgia, D. M. de Leeuw, Electronic transport in field-effect transistors of sexithiophene, J. Appl. Phys. 96 (2004) 5277-5283.

[33] E. Calvetti, L. Colalongo, Zs. M. Kovacs-Vajna, Organic Thin Film Tran-

sistors: a DC/Dynamic model for Circuit Simulation, Solid-State Electron. 49 (2005) 567-577.
[34] F. Torricelli, Z.M. Kovács-Vajna, L. Colalongo, A charge-based OTFT model for circuit simulation, IEEE Trans. Electron Devices 56 (2009) 20-30.
[35] C. Erlen, P. Lugli, Analytical Model of Trapping Effects in Organic Thin-Film Transistors, IEEE Trans. Electron. Devices 56 (2009) 546-552.
[36] F. Torricelli, K. O'Neill, G.H. Gelinck, K. Myny, J. Genoe, E. Cantatore, Charge transport in organic transistors accounting for a wide distribution of carrier energies - Part II: TFT Modeling, IEEE Trans. Electron Devices 59 (2012) 1520-1528.
[37] P. V. Necliudov, M. S. Shur, D. J. Gundlach, T. N. Jackson, Modeling of organic thin film transistors of different designs, J. Appl. Phys. 88 (2000) 6594-6597.
[38] R. L. Hoffman, A closed-form DC model for long-channel thin-film transistors with gate voltage-dependent mobility characteristics, Solid-State Electron. 49 (2005) 648653.
[39] M. Estrada, A. Cerdeira, J. Puigdollers, L. Resendiz, J. Pallares, L.F. Marsal, C. Voz, B. Iñiguez, Accurate modeling and parameter extraction method for organic TFTs, Solid-State Electron. 49 (2005) 1009-1016.
[40] M. Fadlallah, W. Benzarti, G. Biliot, W. Eccleston, D. Barclay, Modeling and characterization of organic thin film transistors for circuit design, J. Appl. Phys. 99 (2006) 104504.
[41] M. Estrada, I. Mejia, A. Cerdeira, J. Pallares, L.F. Marsal, B. Iñiguez, Mobility model for compact device modeling of OTFTs made with different materials, Solid-State Electron. 52 (2008) 787794.
[42] V. Vaidya, J. Kim, J. N. Haddock, B. Kippelen, D. Wilson, SPICE Optimization of Organic FET Models Using Charge Transport Elements, IEEE Trans. Electron Devices 56 (2009) 38-42.
[43] O. Marinov, M. J. Deen, U. Zschieschang, H. Klauk, Organic Thin-Film Transistors: Part I-Compact DC Modeling, IEEE Trans. Electron Devices, 56 (2009) 2952-2961.
[44] F. Zanella, N. Marjanović, R. Ferrini, H. Gold, A. Haase, A. Fian, B. Stadlober, R. Müller, J. Genoe, H. Hirshy, A. Drost, M. König, K.-D. Lee, J. Ring, R. Prétôt, C.C. Enz, J.-M. Sallese, Design and modeling of self-aligned nano-imprinted sub-micrometer pentacene-based organic thin-film transistors, Organic Electron. 14 (2013) 27562761.
[45] C.-H. Kim, Y. Bonnassieux, G. Horowitz, Compact DC Modeling of Organic Field-Effect Transistors: Review and Perspectives, IEEE Trans. Electron Devices 61 (2014) 278-287.
[46] S. Jacob, M. Benwadih, J. Bablet, I. Chartier, R. Gwoziecki, S. Abdinia, E. Cantatore, L. Maddiona, F. Tramontana, G. Maiellaro, L. Mariucci, G. Palmisano, R. Coppard, High performance printed N and P-type OTFTs for complementary circuits on plastic substrate, 42nd European Solid-State Device Research Conference (2012) 173-176.
[47] A. Cerdeira, M. Estrada, R. Garca, A. Ortiz-Conde, and F. J. García-Sánchez, New procedure for the extraction of basic a-Si:H TFT model parameters in the linear and saturation regions, Solid-State Electron. 45 (2001) 1077-1080.
[48] F. Torricelli, Charge transport in organic transistors accounting for a wide distribution of carrier energies - Part I: Theory, IEEE Trans. Electron Devices 59 (2012) 1514-1519.
[49] T. Leroux, Static and dynamic analysis of amorphous-silicon field-effect transistors, Solid-State Electron 29 (1986) 47-58.
[50] S.-S. Chen, and J. B. Kuo, An analytical a-Si:H TFT DC/capacitance model using an effective temperature approach for deriving a switching time model for an inverter circuit considering deep and tail states, IEEE Trans. Electron Devices 41 (1994) 1169-1178.
[51] A. Valletta, A. Daami, M. Benwadih, R. Coppard, G. Fortunato, M. Rapisarda, F. Torricelli, L. Mariucci, Contact effects in high performance fully printed p-channel organic thin film transistors, Appl. Phys. Lett. 99 (2011) 233309.
[52] J.J. Brondijk, F. Torricelli, E.C.P. Smits, P.W.M. Blom, and D.M. De Leeuw, Gate-bias assisted charge injection in organic field-effect transistors, Organic Electron. 13 (2012) 1526-1531.
[53] M. Rapisarda, A. Valletta, A. Daami, S. Jacob, M. Benwadih, R. Coppard, G. Fortunato, L. Mariucci, Analysis of contact effects in fully printed p-channel organic thin film transistors, Organic Electron. 13 (2012) 2017-2027.
[54] L. Mariucci, M. Rapisarda, A. Valletta, S. Jacob, M. Benwadih, G. Fortunato, Current spreading effects in fully printed p-channel organic thin film transistors with Schottky source-drain contacts, Organic Electron. 14 (2013) 86-93.
[55] S. Altazin, R. Clerc, R. Gwoziecki, D. Boudinet, G. Ghibaudo, G. Pananakakis, I. Chartier, R. Coppard, Analytical modeling of the contact resistance in top gate/bottom contacts organic thin film transistors, Organic Electron. 12 (2011) 897-902.
[56] F. Torricelli, E. Cantatore, A. Valletta, S. Jacob, M. Benwadih, R. Coppard, G. Fortunato, M. Rapisarda, L. Mariucci, Physically-based compact model of staggered p- and n-type Organic Thin-Film Transistors, 8th International Thin-Film Transistor Conference, Lisbon - Portugal (2012) 116.
[57] S. Abdinia, F. Torricelli, G. Maiellaro, R. Coppard, A. Daami, S. Jacob, L. Mariucci, G. Palmisano, E. Ragonese, F. Tramontana, A.H.M. Van Roermund, and E. Cantatore, Variation-based design of an AM demodulator in a printed complementary organic technology, Organic Electron. 15 (2014) 904-912.
[58] J.A. Jiménez Tejada, J.A. López Villanueva, P.L. Varo, K.M. Awawdeh, and M.J. Deen, Compact Modeling and Contact Effects in Thin Film Transistors, IEEE Trans. Electron Devices 61 (2014) 266-277.
[59] F. Torricelli, M. Ghittorelli, L. Colalongo, Z.M. Kovács-Vajna, Single-transistor method for the extraction of the contact and channel resistances in organic field-effect transistors, Appl. Phys. Lett. 104 (2014) 093303.
[60] H. Klauk, M. Halik, U. Zschieschang, G. Schmid, W. Radlik, and W. Weber, High-mobility polymer gate dielectric pentacene thin film transistors, J. Appl. Phys. 92 (2002) 52595263.
[61] J. Veres, S. D. Ogier, S. W. Leeming, D. C. Cupertino, and S. M. Khaf- faf, Low-k insulators as the choice of dielectric in organic field-effect transistors, Adv. Funct. Mater. 13 (2003) 199204.